JOURNAL OF SPACECRAFT AND ROCKETS
Vol. 36, No. 5, September–October 1999

Engineering-, Intermediate-, and High-Level Aerodynamic Prediction Methods and Applications

Marnix F. E. Dillenius, Daniel J. Lesieutre, Martin C. Hegedus, Stanley C. Perkins Jr.,
John F. Love, and Teresa O. Lesieutre
Nielsen Engineering and Research, Inc., Mountain View, California 94043

Descriptions and applications of engineering-, intermediate-, and high-level missile aerodynamics prediction methods are presented. The engineering-level method is represented by an experimental data-based code, the intermediate-level method includes enhanced panel method-based codes and a modified linear theory code, and the high-level methods include a space-marching Euler flow solver. All of the methods contain fin and body vorticity models. The engineering- and intermediate-level methods are applied to the prediction of high-angle-of-attack pitch plane and lateral aerodynamic characteristics of missiles at arbitrary roll angle, to aerodynamic loads acting on conventional and chined body shapes, and to assess effects of fin-body gap on fin loads. The intermediate-level methods are also employed in the design of nonconventional fin planforms for minimum hinge moment. The Euler flow solver is applied to the prediction of rolling moments acting on a canard configuration. Comparisons with experimental data are presented. The conclusion is made that the missile aerodynamicist and/or designer should be aware of the availability and should make use of the various levels of missile aerodynamics prediction methodology.

Nomenclature

CA, C_A = axial force coefficient, positive aft along x direction; axial force/$q_\infty S_{\text{REF}}$
C_{BM} = lifting-surface bending moment coefficient, positive side edge up; bending moment/$q_\infty S_{\text{FIN}} L_{\text{REF}}$
C_{HM} = lifting-surface hinge moment coefficient, positive leading edge up; hinge moment/$q_\infty S_{\text{FIN}} L_{\text{REF}}$
C_l = rolling moment coefficient, positive right wing down (clockwise when viewed from rear); rolling moment/$q_\infty S_{\text{REF}} L_{\text{REF}}$

Marnix F. E. Dillenius received his B.S. (with honors), M.S., and Ph.D. degrees in mechanical engineering from the University of California, Berkeley, in 1962, 1964, and 1968, respectively. In 1969, he joined Nielsen Engineering and Research (NEAR), where he was involved in modeling aerodynamic interference, standard takeoff and landing aerodynamics, and trailing-wake vortex studies. He originated and/or made major contributions to analytical investigations concerning supersonic wing loading theories, external store separation characteristics, and detailed missile aerodynamic prediction methods. Dr. Dillenius has been president of NEAR since 1992. He is an Associate Fellow of the AIAA.

Daniel J. Lesieutre received his B.S. and M.S. degrees in aeronautical and astronautical engineering from Purdue University in 1983 and 1985, respectively. Since joining NEAR, he has directed research in applied aerodynamics, aerodynamic shape optimization, aeroelastic fin design, and unsteady aerodynamics. He has participated in projects involving hydrodynamics, missile, aircraft and launch vehicle aerodynamics, and store separation. He has successfully demonstrated the use of numerical optimization methods for the multidisciplinary design of control fins with geometric and structural constraints. He is a Senior Member of the AIAA.

Martin C. Hegedus received his B.S. degree in 1990 from the University of California, Davis, and an M.S. in aeronautics and astronautics from Stanford University in 1992. Since joining NEAR in 1994, he has worked on the development of aerodynamic and store separation prediction codes and graphical user interfaces. He has made contributions to several aerodynamic prediction codes and has assisted in the analysis of the aerodynamic and separation characteristics of several commercial launch vehicles. Mr. Hegedus is responsible for the development of the NEAR Event Manager, a software library for the integration and management of distributed software modules. He is a Senior Member of the AIAA.

Received 4 June 1997; revision received 5 January 1999; accepted for publication 29 January 1999.

CM, C_M = pitching moment coefficient, positive nose up; vector along y axis; pitching moment/$q_\infty S_{REF} L_{REF}$
CN, C_N = normal force coefficient, positive up along z axis; normal force/$q_\infty S_{REF}$
C_{NF} = lifting-surface normal force with S_{REF} = lifting-surface planform area
Cn, C_n = yawing moment coefficient, positive nose to right; vector along negative z axis; yawing moment/$q_\infty S_{REF} L_{REF}$
C_p = pressure coefficient, $(p - p_\infty)/q_\infty$
CY, C_Y = side force coefficient, positive to right along y axis; side force/$q_\infty S_{REF}$
c_R = lifting-surface root chord
d = body diameter
L_{REF} = reference length
M_∞ = freestream Mach number
p = static pressure, lb/ft^2
p_∞ = freestream static pressure, lb/ft^2
q_∞ = dynamic pressure of freestream, $0.5\rho_\infty V_\infty^2$, lb/ft^2
S_{FIN} = lifting-surface planform area, ft^2
S_{REF} = reference area, ft^2
V_∞ = freestream velocity, ft/s
x, y, z (or X, Y, Z) = body-fixed (rolled) coordinates; x, positive aft; y, positive to right; z, positive up
x_{cp} = axial coordinate of center of pressure, measured from the lifting-surface root chord leading edge
x_m = axial coordinate of moment center, positive aft
α = angle of attack or pitch, deg
α_c = included angle of attack, angle between freestream vector and body centerline, deg
β = angle of sideslip, deg; positive wind from right
δ_p = pitch-control deflection angle
δ_r = roll-control deflection angle
λ = fin taper ratio
ϕ = roll orientation angle, positive right wing down

Introduction

MISSILE aerodynamics differs from airplane aerodynamics in many ways. There are large differences between missile and aircraft geometries and in the flow conditions typically encountered by each type of vehicle. In the future these differences may be less pronounced. Conventional missile geometries can be characterized by long, slender bodies with one or more low-aspect-ratio fin sets. Conventional aircraft exhibit medium-to-large-aspect-ratio wings and smaller span horizontal stabilizer surfaces. Even at low angles of attack, the canard-tail vortical interference on a missile is stronger than the wing-tail interference on conventional aircraft. Future missile configurations may include noncircular or blended-body cross sections and nonconventional fin planforms.

The flow conditions encountered by a maneuvering missile during an air-to-air (or other) mission profile can include high angles of attack; nonzero angle of roll; fin deflections for pitch, yaw, and roll control; rotational rates; a wide range of flight Mach numbers; and variation in altitude. The high angle-of-attack flow condition gives rise to formation of flow separation vortices from the fins and the body. All of the vorticity travels aft along the missile configuration and influences the overall and component loads in a nonlinear fashion. Transonic and high supersonic flight conditions also bring nonlinear effects. For cases involving angle of attack and angle of roll (or angle of pitch and angle of sideslip), there will be coupling of the pitch plane and lateral aerodynamic effects. When vortices are present, these coupling effects become very nonlinear and difficult to predict.

For the reasons just mentioned, any missile aerodynamics prediction method should as a minimum contain modeling or simulation of the nonlinear effects of vortices as they stream aft along the missile. The methodology should handle asymmetric flow conditions associated with nonzero roll angle and asymmetric fin deflections (for example, roll control). Missile aerodynamics prediction methods should be able to model low-aspect-ratio lifting surfaces or fins with the associated leading-edge vortical effects and lift augmentation. Fin-on-fin and fin-on-body aerodynamic interference must

Stanley C. Perkins Jr. received a B.S. degree in mechanical engineering from the University of Rochester in 1973 and an M.S. degree in applied mechanics from Stanford University in 1974. Since joining NEAR in 1974, he has worked in a variety of areas, including the development and application of panel methods and engineering models to transport and fighter aircraft and missiles, high-angle-of-attack aerodynamics, the prediction of store separation characteristics from fighter aircraft, the analysis of trajectories of surface- and underwater-launched configurations, the development of a workstation-based capability for predicting post-intercept trajectories of missile debris fragments, and the modeling and hydrodynamic analysis of submersible vehicles undergoing steady and unsteady maneuvers. He is a Senior Member of the AIAA.

John F. Love received his B.S. in aerospace engineering in January 1989 from the University of Kansas, Lawrence, where he won 1st Place in the AIAA Team Aircraft Engine Design Competition. After graduation, he worked as a structural design and analysis engineer for a launch vehicle company and later for a space and communications company. He received his M.S. in aeronautical engineering from the California Polytechnic State University, San Luis Obispo. Since joining NEAR as a research engineer in 1995, he has worked on missile and launch vehicle aerodynamic prediction and analysis, wind-tunnel data analysis, and software maintenance of NEAR's aero-prediction programs.

Teresa Lesieutre received her B.S. degree in aerospace engineering from the State University of New York, Buffalo, in 1988 and her M.S. degree in mechanical engineering from San Jose State University in 1996. During her employment at NEAR, she has participated in projects involving submersible hydrodynamics, missile and launch vehicle aerodynamics, store separation, and aerodynamic and aeroelastic optimization of missile fins. She is a Member of the AIAA.

be included. For cases involving high flight Mach numbers, the prediction methods may need to account for nonlinear compressibility effects associated with the body such as the influence of the body nose shock on the forward fins. In extreme cases involving high angle of attack and with the fins in the 45-deg roll position, the flow between the lower fins may be choked. This is another nonlinear compressibility phenomena. In addition, fin-stall effects are important at high angles of attack.

Today the missile aerodynamicist has a choice of a fair number of aerodynamic prediction methods. Status and developmental plans associated with engineering-level prediction methods NSWC AP95 and Missile DATCOM are described in Refs. 1 and 2. The methods available today may not address all of the capabilities and nonlinear phenomena already listed. Engineering-level methods based on experimental data inherently include nonlinear effects at least to the extent set by the actual model shape and scale employed. Panel methods by themselves do not model vortical effects associated with flow separation but can predict aerodynamics of conventional aircraft (high-aspect-ratio wing, small tail surfaces) fairly well because vortical interference may not be so important. In contrast, standard panel methods are not adequate for predicting missile aerodynamics, which is very much influenced by vortical effects. Panel method-based methods are convenient in that the details of the body and fin shapes can be handled relatively easily. Intermediate-level approaches, as defined herein, are methods based on linear theory (including panel methods) and enhanced to model vortical effects and possibly nonlinear compressibility. Transonic and high supersonic flight Mach numbers are not predicted well by the intermediate methodology described in this paper. Apart from the experimental data-based methods, these flow conditions typically require high-level methods provided by computational fluid dynamics (CFD). In general, CFD approaches require considerable computer resources and code user's expertise. However, the NEARZEUS space-marching Euler flow solver[3] mentioned in the following paragraphs is sufficiently easy to use and runs fast on workstations. The VECC code, based on impact theory,[4] can provide engineering-level or preliminary estimates of aerodynamics acting on supersonic/hypersonic flight Mach-number vehicles with arbitrary shapes.

So far the comments in this introduction have dealt with steady aerodynamics. For cases involving angle of attack and sufficiently high rotational rates, effects caused by vortex lag will result in time-dependent aerodynamic characteristics. In such cases unsteady vortex tracking schemes are required; an example is the SHAMAN code,[5] which is based on intermediate-level methodology augmented with a true unsteady vortex tracking scheme. On a higher level still, unsteady CFD solutions can be applied to cases warranting full unsteady flow analyses. This paper addresses only steady or quasi-steady missile aerodynamic prediction.

In what follows, references are made to aerodynamics prediction computer programs developed, modified, or in use over the years at Nielsen Engineering and Research (NEAR). The engineering-level category is represented by missile aerodynamics prediction code M3HAX.[6] The intermediate-level category is represented by panel method-based codes SUBDL (previously designated SUBSAL[7]) and SUPDL (previously designated NSWCDM[8]) for aerodynamic force distributions acting on subsonic and supersonic configurations, respectively, and the forebody vortex shedding code (VTXCHN[9]). The high-level category is represented by the NEARZEUS space-marching Euler solver.[3] All of these are summarized in the technical approach. These codes are applied singly or in combination with other codes to a variety of missile aerodynamics predictions, fin-on-body gap effects, and fin planform optimization (OPTMIS). Additional examples, including missile launch from a pitching aircraft at high angle of attack, are described in Ref. 10.

For the sake of comparison, some results obtained with the AP95 and Missile DATCOM (MISDAT) codes are included in the prediction of fin-on-body aerodynamics described in this paper. There are additional experimental database/simple analytical theory methods for missile aerodynamics in use by companies worldwide; for example, British Aerospace Sowerby Research Center has its proprietary code, as do Aerospatiale and Matra Defense in France, and MBB and Dornier (now DASA) in Germany.

Technical Approach

Short descriptions of the M3HAX, SUBDL/SUPDL, VTXCHN, NEARZEUS/ZEUSBL, and OPTMIS codes are given below. Further details can be found in the cited references.

M3HAX

An engineering-level prediction method has been developed for aerodynamic performance prediction and for preliminary design of conventional missiles with cruciform fin sections.[6,11] The method uses the Triservice systematic fin-on-body force and moment database,[11,12] which covers a Mach number range from 0.6 to 4.5, fin aspect ratios from 0.25 to 4.0, taper ratio from 0.0 to 1.0, angles of attack up to ±45-deg arbitrary roll angles, and deflection angles from −40 to 40 deg. The prediction method uses the equivalent angle-of-attack concept that includes the effects of vorticity, geometric scaling, and nonlinear body-flow effects for high Mach numbers. The latest program described here is designated M3HAX.[6] Program M3HAX has been developed by extending the M3F3CA code[11] to angles of attack up to 90 deg and by including rotational-rate effects and nonuniform flowfield effects. Reference 6 summarizes the experimental and analytical databases included in the M3HAX program and describes the equivalent angle-of-attack methodology including the inclusion of rotational-rate and nonuniform flow effects. Extensive comparisons to independent experimental data for a variety of configurations and flow conditions are also presented in Ref. 6; several additional comparisons to experiment are shown in this paper. The range of parameters allowed by program M3HAX is summarized here.

The flow conditions are as follows: $0.5 \le M_\infty \le 5.0$; -90 deg $\le \alpha_c \le 90$ deg ($\alpha_c > 45$ deg by analytical extension); arbitrary roll angle is -40 deg $\le \delta \le 40$ deg; rotational rates (p, q, r); and user-specified nonuniform flowfield. The geometries are as follows: $0.25 \le AR \le 10.0$ ($AR > 4$ by analytical extension); $0.0 \le \lambda \le 1.0$; up to three finned sections; one to four fins per finned section; identical fins within a section; symmetrical airfoil sections; no fins with forward sweep; and no fin trailing-edge sweep.

SUBDL/SUPDL

The SUBDL and SUPDL methods are based on fast-running subsonic horseshoe vortex and supersonic constant u-velocity panel methods, respectively, for modeling up to two fin sections including fin-body mutual interference on an axisymmetric body. Subsonic point sources/doublets or supersonic linearly varying line source/doublet singularities are employed to model the axisymmetric bodies for subsonic and supersonic Mach numbers, respectively. The fin sections can have planar, triform, cruciform, or low-profile fin layouts. Fin planform is arbitrary with the root chord parallel to the body centerline. Body and fin-flow separation vortices are modeled and tracked aft along the configuration. Vortex-induced effects are included in the aerodynamic load analysis. Both fin and body aerodynamic loads include nonlinear augmentations. Simple fin-stall models are incorporated. The SUBDL and the SUPDL methods can handle effects of rotational rates and nonuniform flow, and both codes include a postprocessor for generating distributions of aerodynamic forces for input to the NASTRAN structural analysis program. For high supersonic flight Mach number cases with attached fin leading-edge shocks, program SUPDL contains optional nonlinear pressure calculation methods based on applying two-dimensional shock expansion or Newtonian theory to strips on the lifting surfaces. In this option SUPDL has the capability to account for strip-on-strip and body-on-strip interference by an innovative use of the linear panel solution. Detailed descriptions applicable to the SUBDL and SUPDL codes are available in Refs. 7 (SUBSAL is an earlier version of SUBDL) and 8 (NWCDM-NSTRN is an earlier version of SUPDL), respectively. These codes can be applied to simplified aircraft configurations as well. The ranges of application of the SUBDL and SUPDL codes are listed here. The flow conditions are as follows: 0.1 < Mach < critical; 1.1 < Mach < 2.5 (fin loads up to Mach 6); −20 deg < angle of attack < 20 deg; roll angle arbitrary; −20 deg < fin deflection angle < 20 deg; rotational rates; and user-specified flowfield. The geometries are fin planform and aspect-ratio arbitrary (except root chord parallel to body centerline).

VTXCHN

Computer code VTXCHN is an intermediate-level analytical prediction method for efficient prediction of steady aerodynamic loads acting on forebodies under the influence of shed vortices. The shed vortices form a vortex cloud. VTXCHN has been integrated into the conceptual design aerodynamic prediction method HASC (high-angle-of-attack stability and control)[13] and in the comprehensive store separation analysis program STRLNCH.[14] The forebodies may have arbitrary cross sections with or without corners or sharp chine edges. Flow conditions include subsonic flow up to the critical speed, high angle of attack, angle of sideslip, and steady rotational rates. VTXCHN combines conformal transformation of the body cross section to the circular or mapped plane and elements of linear theory with models for the nonlinear effects of primary vortex shedding. The calculation procedure involves marching down the forebody from one cross section to the next, performing flow analyses in the mapped plane, and calculating aerodynamic loadings in the physical plane.

NEARZEUS/ZEUSBL

The NEARZEUS code[3] is a space-marching Euler solver that combines a semiautomatic, multiple zone, gridding technique and a second-order extension of Godunov's method. The Godunov method[15] is an upwind scheme based on the Riemann problem for steady supersonic flow. It is cast in control volume form and consists of a predictor and corrector step. The predictor step advances the primitive variables using Euler's equations in nonconservation form. Derivatives are computed using a limited central-differencing procedure. The corrector step modifies Godunov's method by assuming linear property variations within each control volume. Because the flow must remain supersonic in the axial direction, the flow conditions are typically limited to Mach numbers greater than 2.0 and angles of attack less than 30 deg.

The original ZEUS code[16] was extended to very high Mach numbers[17] by incorporating the high-temperature effects of air in chemical equilibrium. These effects are accounted for by using curve fits to compute thermodynamic properties of equilibrium chemically reacting air.

A boundary-layer module, ZEUSBL,[3,18] contains an integral boundary-layer method designed specifically to be used in tandem with the NEARZEUS code. It is based on the MEIT code,[19] which was originally designed for re-entry vehicles. Special procedures are included to account for transition and shock-boundary-layer interaction.

The NEARZEUS/ZEUSBL codes run on workstations; are robust and capable of treating realistic configurations efficiently and accurately; and together provide a means to obtain estimates of local skin friction, heat transfer, and skin-friction drag in addition to the overall aerodynamic loads. The real gas capability can provide accurate predictions in support of future hypersonic aircraft. Considering the high cost of wind-tunnel testing and of performing Navier–Stokes calculations, the NEARZEUS/ZEUSBL codes provide an economical predictive tool that is not dependent on a database and that includes nonlinear aerodynamic effects, which are typically missing in simpler methods. Run times on an HP 9000/735 workstation are of the order of 15 s for a simple body-alone configuration and under a minute for a body-canard-tail configuration at a high Mach number and including real gas effects. To date, NEARZEUS/ZEUSBL codes have been installed on the following computer platforms: SunSPARC, HP 9000/700 series, IBM 6000 IAX, SGI Indigo R4000/Elan, and Alpha/VMS AXP.

OPTMIS

NEAR has developed an innovative design tool employing combined numerical optimization and aerodynamic/structural prediction techniques for the optimal aerodynamic design of missile configurations with geometric constraints such as those imposed by conformal/internal carriage. The Planform/Configuration Optimization Program OPTMIS[20] for arbitrary cross-section bodies with up to two fin sections was developed under an Air Force SBIR Contract. A brief description of the methodology employed is given; further details can be found in Ref. 20. The Results section in this paper describes one of the developed optimized fin planforms verified by wind-tunnel testing and Navier–Stokes CFD calculations.

A modular numerical optimization shell was developed and coupled with subsonic and supersonic fast-running panel method-based missile aerodynamic prediction programs that include nonlinear high-angle-of-attack vortical effects. The combined methods have been used to demonstrate the numerical optimization procedure for missile fin optimization with several different design objectives and with several different geometric constraints. Details are given in Ref. 20. The design variables govern fin planform shape. For aerodynamic design problems related to missile fins, the desired objective is generally a nonlinear function of the design variables. In addition, various forms of the objective function can be specified depending on the desired design goal, and several constraints may need to be imposed on the chosen design variables.

The optimization algorithm implemented in the OPTMIS program is Powell's Conjugate Directions Method (PCDM).[20–22] NEAR subsonic and supersonic panel method-based aerodynamic prediction modules, SUBDL[7] and SUPDL,[8,23] are employed as the aerodynamic prediction modules within the design code. The VTXCHN[9] methodology is used to model circular and noncircular body shapes within the SUBDL and SUPDL modules.

The optimization method solves a minimization problem. An Index of Performance (IP) is defined, which contains both the design objectives and constraints. The Sequential Unconstrained Minimization Technique (SUMT) of Fiacco and McCormick[24] does this by defining an augmented objective function expressed as an IP, which is minimized during the optimization procedure. Details of the optimization procedure employed can be found in Ref. 20.

Selected Results

Some representative results including comparisons between predictions obtained with the engineering-level, intermediate-level, and high-level prediction methods already described and wind-tunnel data are given below. Aerodynamic predictions for different missile models are compared to experiments including pitch-plane and lateral-aerodynamic characteristics. Aerodynamic characteristics of circular and chined cross-section bodies at high angles of attack under the influence of body vorticity are presented without and with effects of angle of sideslip. Pitch-plane characteristics predicted for a nonconventional body-wing vehicle are compared with wind-tunnel data. The predicted effects of fin-body gap on fin aerodynamic characteristics are compared with experiment. Predicted rolling moments acting on a two-fin canard section with fixed cant angles are compared with experimental data. The results of a fin planform optimization scheme aimed at minimizing the axial travel of center of pressure are described including results from a wind-tunnel test.

Aerodynamic Characteristics of Two-Fin Set Missile Configurations

In the following sections comparisons of predicted results and wind-tunnel data are presented for both canard-tail and wing-tail missile configurations.

AIM-9L Longitudinal Characteristics

Figure 1 shows normal force and pitching moment coefficient acting on the unrolled wind-tunnel model of the AIM-9L, shown at the top of Fig. 1, for angles of attack up to 20 deg. The Mach number is 0.4, and results are plotted for the horizontal canard fins set at zero and 10 deg for nose-up pitch control. The experimental data[25] show a fair amount of nonlinearity, which is caused by the canard fins stalling at relatively low angle of attack and by the induced effects of the canard-fin wake interference on the tail fins. The induced effects are the main reason for the normal force being essentially invariant but the pitching moment showing the effects of pitch control at low angles of attack. These characteristics, including the effect of pitch control, are predicted well by SUBDL.

TF-4 Longitudinal Characteristics

Figure 2 presents overall normal force and pitching moment coefficients as a function of angle of attack for a TF-4 wind tunnel model.[26] The canards can be deflected for control. Experimental

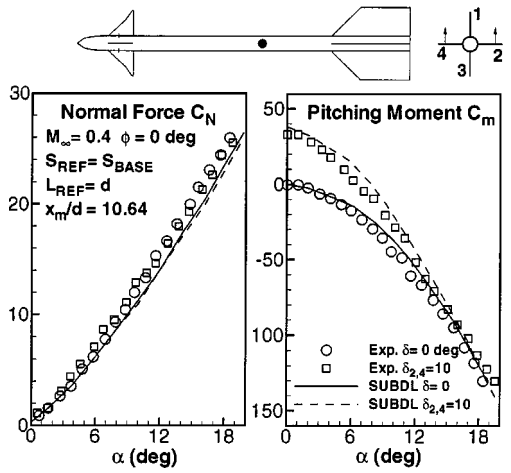

Fig. 1 Longitudinal aerodynamic characteristics of an AIM 9-L wind-tunnel model with canard pitch control.

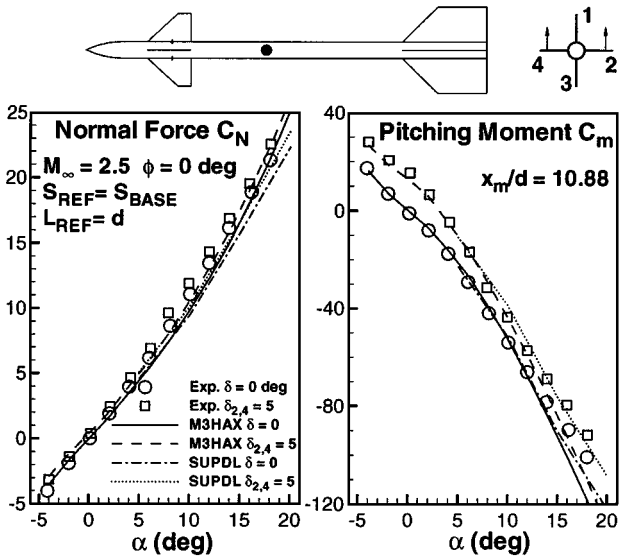

Fig. 2 Longitudinal aerodynamic characteristics of a TF-4 wind-tunnel model with canard pitch control.

results in Fig. 2 are given for the model at 0-deg roll angle and for the horizontal canards deflected 0 and 5 deg (leading edge up) for pitch control. The Mach number is 2.5. Predicted results from both the M3HAX and SUPDL codes are compared with the wind-tunnel results in Fig. 2. Normal force is predicted well by both codes throughout the angle-of-attack range although it is somewhat underpredicted by the SUPDL code at the higher angles. In regard to pitching moment, SUPDL results compare well throughout the angle-of-attack range whereas the M3HAX results indicate a pitching moment at the higher angles, which is more nose down than the data. A small error in the distribution of loads on the long afterbody or large tail fins could explain this difference.

TF-4 Rolling Moment Characteristics

Rolling moment coefficients are shown in Fig. 3 for angles of attack up to about 20 deg for the canard control wind-tunnel model[26] shown at the top of Fig. 3 at roll angle 26.6 deg. The horizontal canard fins are differentially deflected 5 deg for roll control. Results are displayed for Mach 1.75 and 2.5. For angle of attack up to 10 deg, the canard fin wakes swirl along the body aft of the canard section and induce highly nonlinear effects on the tail fins. The overall rolling moment C_l is heavily influenced by the vortical wakes from the canards, which can be seen from the difference between the tail fins off and tail fins on results. In addition, at angle of attack above 10 deg, the long section of body between the canard section and the tail section sheds body-flow separation vortices. As a result, at Mach

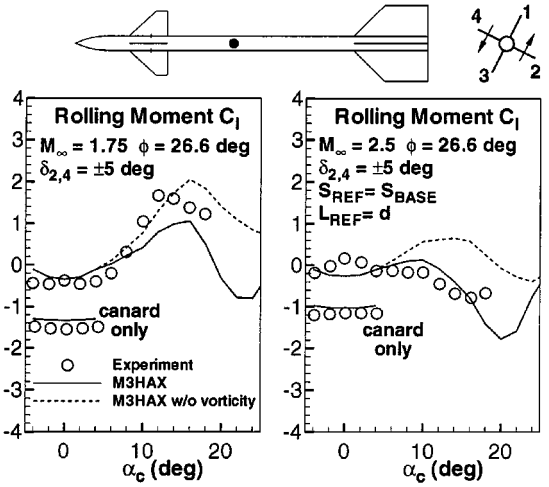

Fig. 3 Rolling moment coefficient of a TF-4 wind-tunnel model with canard roll control.

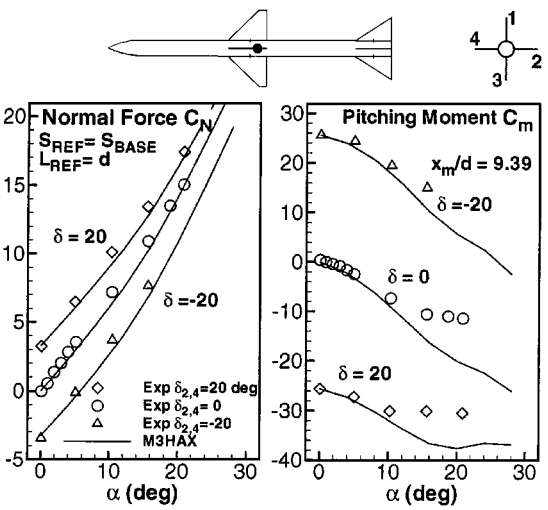

Fig. 4 Longitudinal aerodynamic characteristics of a Sparrow wind-tunnel model with tail pitch control; M_∞ = 1.6 and ϕ = 0 deg.

1.75 the combined effects cause the canard rolling moment to be nearly negated at zero angle of attack. The overall rolling moment then turns positive, after which it starts dropping back toward zero. The Mach 2.5 data also show the negation at zero angle of attack. Above this angle the overall rolling moment approaches the tail fins off (canard rolling moment) result before turning to zero at 20 deg. The M3HAX code shows the same trends and actually predicts the magnitudes fairly well for these difficult cases.

Sparrow with Tail Control, Longitudinal Characteristics

Figure 4 shows normal force and pitching moment coefficients as a function of angle of attack for a Sparrow wind-tunnel model.[27] The tail fins can be deflected for control. Experimental results are given for 20-, 0-, and −20-deg pitch control provided by the horizontal tail fins with the model at zero roll angle. Mach number is 1.6. Predictions obtained with the M3HAX code are indicated by the solid lines. The predicted and measured normal force coefficients compare well throughout the range of angle of attack. The pitching moment coefficients appear to be underestimated by M3HAX for angles of attack above 10 deg. A slight error in the nose loads may account for this discrepancy.

Sparrow Tail Control, Tail Fin Aerodynamic Characteristics

The tail fin loads corresponding to the overall longitudinal characteristics just described are shown in Fig. 5. The agreement in fin normal force, hinge moment, and root-bending moment between M3HAX predictions and experiment can be considered good to excellent. The aerodynamic loads acting on the horizontal tail

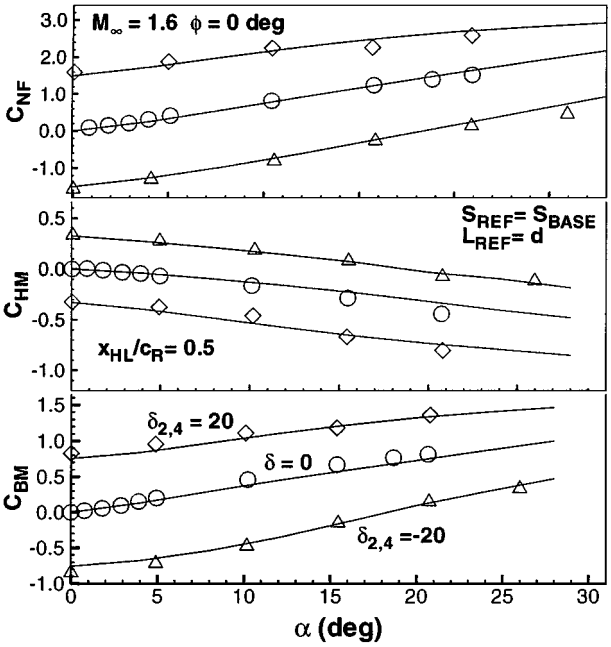

Fig. 5 Tail fin force and moment coefficients of a Sparrow wind-tunnel model with tail pitch control.

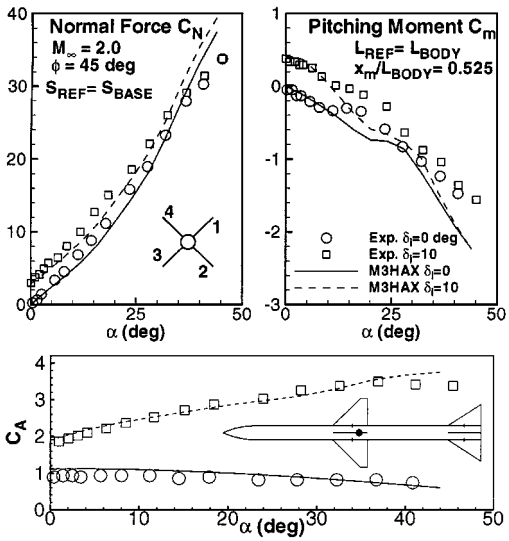

Fig. 6 Longitudinal aerodynamic characteristics of a Sparrow wind-tunnel model with wing pitch control.

surfaces are influenced by the vortical wakes from the forward horizontal wing surfaces.

Sparrow with Wing Control, Longitudinal Characteristics

The bottom of Fig. 6 shows the wing control version of a Sparrow wind-tunnel model.[28] The model is rolled 45 deg, and all four wing panels can be deflected for pitch control. Overall normal force, pitching moment, and axial force coefficients are shown in Fig. 6 for 0- and 10-deg pitch control as a function of angle of attack. Mach number is 2.0. In this case the vortical wake affecting the tail fin loads includes vortical effects from all four wing panels. The effect of wing pitch control on normal force is predicted fairly well up to about a 35-deg angle of attack. The experimental pitching moment shows a nonlinear behavior between 14- and 22-deg angle of attack, more so for the zero-wing pitch control condition than for the 10-deg pitch control condition. The M3HAX predictions indicate the same behavior shifted to higher angles of attack. Above 30 deg the prediction underestimates the pitching moment. Measured and predicted axial force coefficients are in good agreement for the 0- and 10-deg pitch control conditions throughout the range of angle of attack.

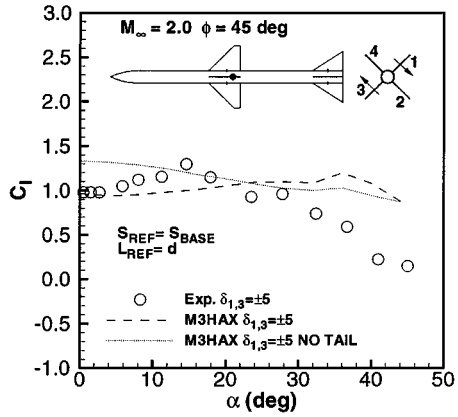

Fig. 7 Rolling moment coefficient of a Sparrow wind-tunnel model with wing roll control.

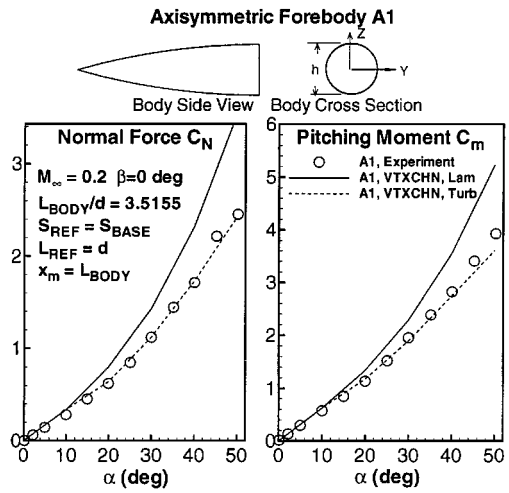

Fig. 8 Longitudinal characteristics of forebody A1.

Sparrow Wing Control, Rolling Moment

Figure 7 shows the overall rolling moment with the right upper wing (panel 1) and left lower wing (panel 3) deflected 5 deg for roll control. The model is rolled 45 deg as for the case already described. For this roll control condition the experimental rolling moment displays nonlinear behavior with angle of attack. Predictions obtained with the M3HAX code are provided with and without tail fins. At low angles of attack the negation effect of the tail fins predicted by M3HAX is similar to that shown for the TF-4 model described earlier. The level in magnitude of the overall rolling moment is predicted reasonably well by M3HAX up to about 25-deg angle of attack.

Circular Cross Section and Chined Body-Alone Aerodynamics

Axisymmetric Forebody, A1

Figure 8 shows the longitudinal characteristics predicted by VTXCHN for a three-caliber axisymmetric forebody. For smooth bodies VTXCHN can use either a laminar or turbulent flow separation model. Both the laminar and turbulent results are shown in Fig. 8. The Reynolds number of the experiment,[29] based on base diameter, is 4×10^5, which is in the transition region. VTXCHN's turbulent results agree very well with experiment. The pressure distribution halfway down the body is shown in Fig. 9 for angles of attack of 10 and 30 deg. At 10-deg angle of attack agreement between VTXCHN prediction and data is good for either laminar or turbulent separation criteria. At 30 deg the predicted pressures based on the turbulent criteria agree better with experiment than those obtained with the laminar criteria. Generally, VTXCHN captures the details of the pressure distribution to first order, but higher-order effects such as those caused by secondary separation and reattachment are not modeled by the present version of VTXCHN. For cases with sideslip at 10- and 30-deg angles of attack, Figs. 10 and 11, respectively, the agreement in the lateral characteristics is good at 10 deg and is fair

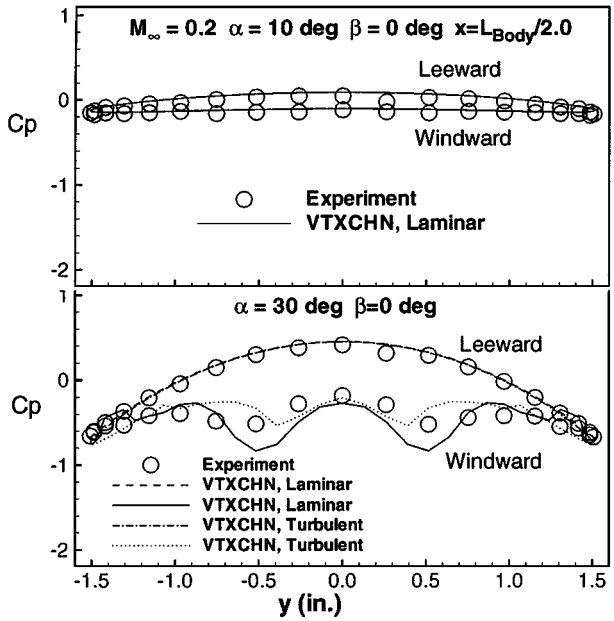

Fig. 9 Pressure distribution on forebody A1 for $\alpha = 10.0$ and 30.0 deg.

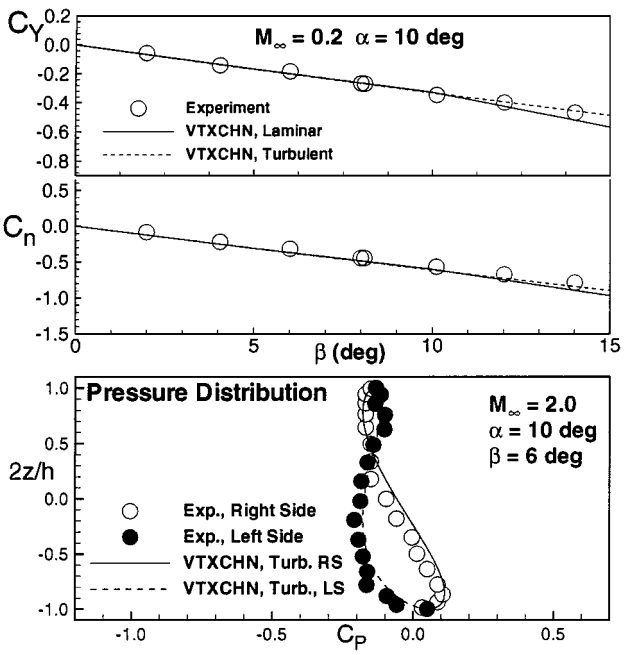

Fig. 10 Lateral characteristics of forebody A1; $M_\infty = 0.2$ and $\alpha = 10.0$ deg.

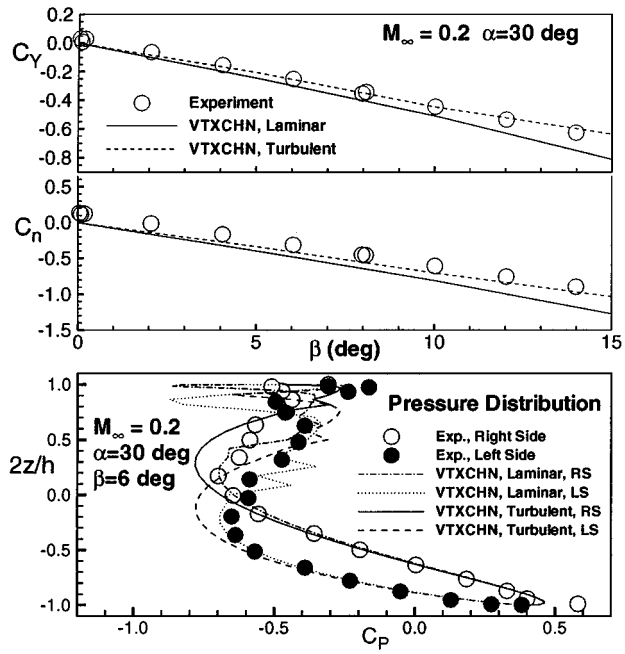

Fig. 11 Lateral characteristics of forebody A1; $M_\infty = 0.2$ and $\alpha = 30.0$ deg.

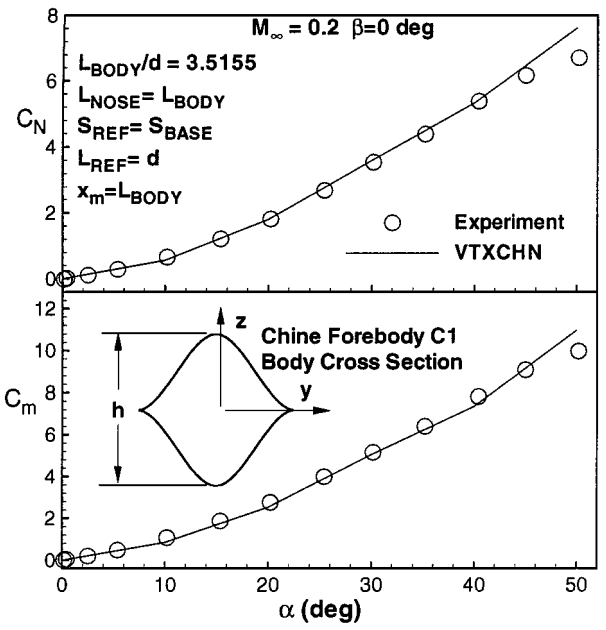

Fig. 12 Longitudinal characteristics of chine forebody C1.

at 30 deg. It is likely that asymmetric vortex shedding relative to the crossflow velocity occurs at angles of attack of 30 deg and higher. Asymmetric vortex shedding at high angle of attack at zero sideslip currently is not modeled by VTXCHN.

Examples of pressure distributions for a 6-deg angle of sideslip are also shown in Figs. 10 and 11 for an axial location halfway down the forebody. Note that the pressure coefficients are plotted against the vertical coordinate parameter $2Z/h$. At an angle of attack of 10 deg, the laminar and turbulent predictions are nearly identical and agree very well with the data. At 30-deg angle of attack, the VTXCHN predictions agree fairly well on the windward side ($2Z/h$ less than 0.0). Near $2Z/h = 0.0$ the predicted right-side (RS) and left-side (LS) pressure contours cross over. This behavior is indicated by the experimental data. On the leeward side the measured pressures may be influenced by secondary vorticity.

Chine Forebody, C1

Figure 12 presents the longitudinal comparisons for the sharp chine forebody, C1. The predicted results are based on forced separation at the edges and compare well with experiment up to a 45-deg angle of attack. Above this angle the VTXCHN predictions are somewhat high, most likely caused by the vortex cloud (collection of shed vortices) being too close to the upper surface of the body.

The predicted and experimental pressure distributions on the C1 forebody are given in Fig. 13. Agreement is reasonably good for both 10- and 30-deg angles of attack although the pressures on the upper surface near the chine edges are underpredicted.

Figures 14 and 15 display the lateral characteristics for 10- and 30-deg angles of attack, respectively. At 10-deg angle of attack agreement between the prediction and experiment is considered good. The lateral results predicted by VTXCHN at an angle of attack of 30 deg are high and do not exhibit the almost linear characteristics of the experimental data, which may be due to the vortex cloud being washed too close to the side of the body for the flow conditions considered.

Typical pressure distributions around the chine forebody C1 are shown in Figs. 14 and 15 at axial location $L_{\text{body}}/2.0$ for a 6-deg

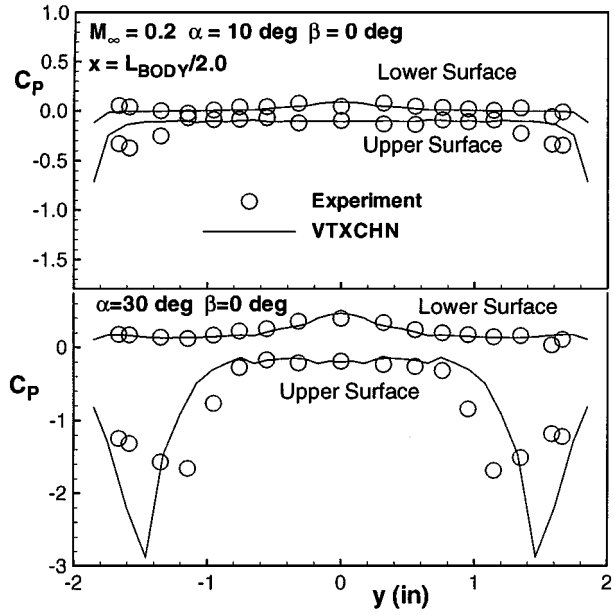

Fig. 13 Pressure distribution on forebody C1 for $\alpha = 10.0$ and 30.0 deg.

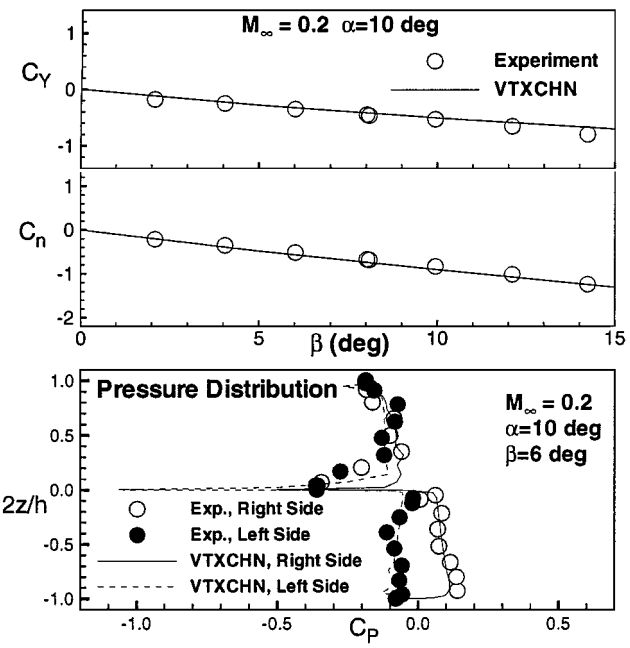

Fig. 14 Lateral characteristics of forebody C1; $M_\infty = 0.2$ and $\alpha = 10.0$ deg.

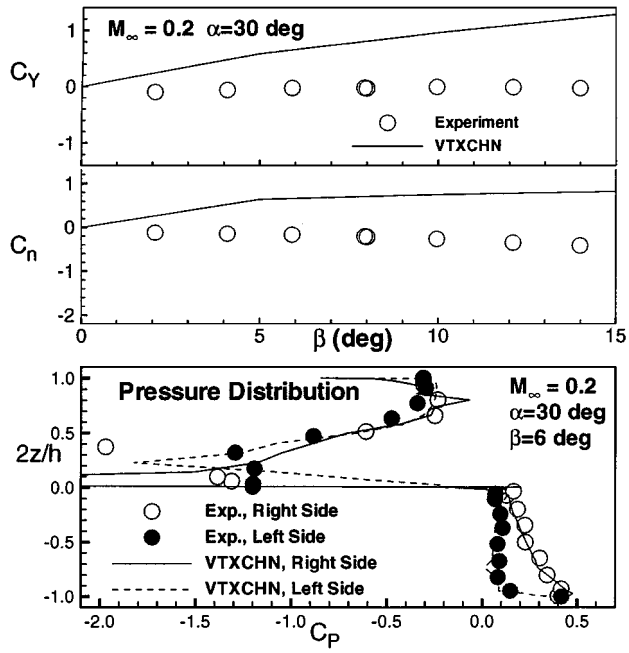

Fig. 15 Lateral characteristics of forebody C1; $M_\infty = 0.2$ and $\alpha = 30.0$ deg.

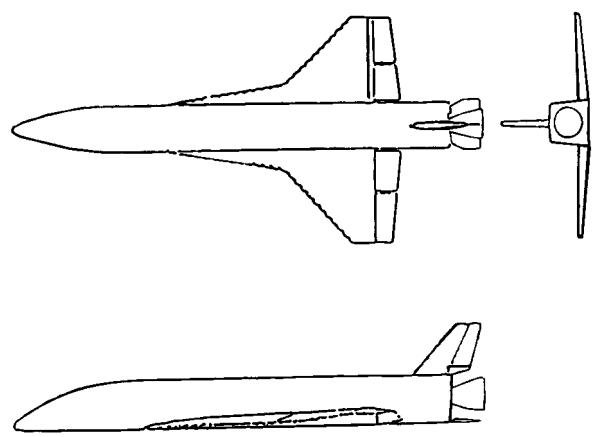

Fig. 16 X34C geometry.

angle of sideslip. The pressure coefficients are plotted against vertical coordinate parameter $2Z/h$ where h is the height of the chine forebody. Figure 14 shows the pressure distribution for a 10-deg angle of attack. The VTXCHN prediction agrees well with the experimental data on both sides of the body except near the chine edges where the pressure is somewhat underestimated. For a 30-deg angle of attack, Fig. 15, the prediction agrees fairly well with experiment except near the chine edges although the major differences between pressures measured on the RS and LS are predicted.

Nonconventional Wing-Body Configuration

The X34C geometry is shown in Fig. 16. The X34C has several geometrical characteristics that make it desirable to use an intermediate- rather than an engineering-level prediction code to predict its aerodynamics. The X34C has a 10-caliber body, drooped nose, noncircular body, leading-edge strake, wing camber, wing incidence angle, wing twist, low wing, inboard and outboard flaperons, and body flap. Figure 17 shows normal-force and pitching-moment coefficient comparisons between wind-tunnel data (private communication, Orbital Sciences Corporation, 1997) and predicted results from the combined VTXCHN/SUBDL codes for the X34C at various subsonic Mach numbers. The predicted normal-force and pitching-moment values compare well to experimental data up to an angle of attack of 15 deg. Past a 15-deg angle of attack, the normal force at Mach 0.95 is overpredicted, and the normal force at Mach 0.40 is underpredicted. The pitching moment at Mach 0.95 past a 15-deg angle of attack is underpredicted. It is interesting to see how well the Mach 0.95 case is predicted although this case is clearly in the transonic regime. The downward shift in the pitching moment at zero normal force and the neutral stability of the vehicle is predicted correctly.

Fin Gap Study Results

An investigation of the unporting effects associated with deflected fins was performed at NEAR. Part of the study was to assess the predictive capability of missile aerodynamic prediction codes for deflected fin forces and moments. An example is shown here for FIN10 of the McDonnell-Douglas/NASA Langley Fin-Body Interference Study.[30] FIN10 mounted on an ogive-cylinder body is depicted in Fig. 18. The forebody will shed flow separation vortices, which will influence the fin loads. The fin has an aspect ratio of $\frac{2}{3}$ and a taper ratio of $\frac{1}{2}$. This fin was chosen because of its small span and low aspect ratio, which will have larger center-of-pressure

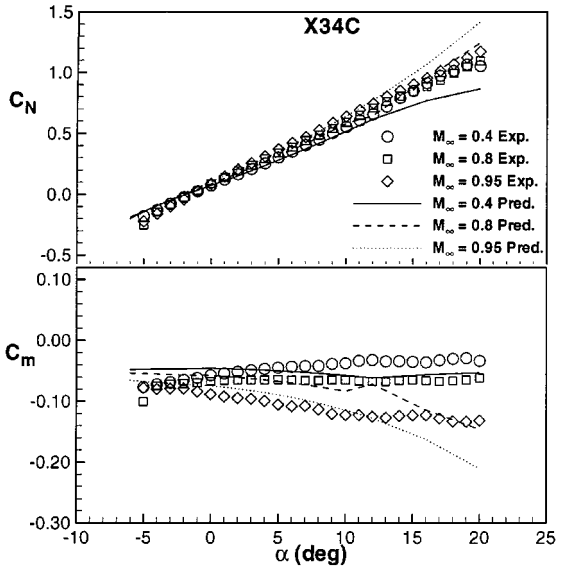

Fig. 17 Longitudinal characteristics of the X34C.

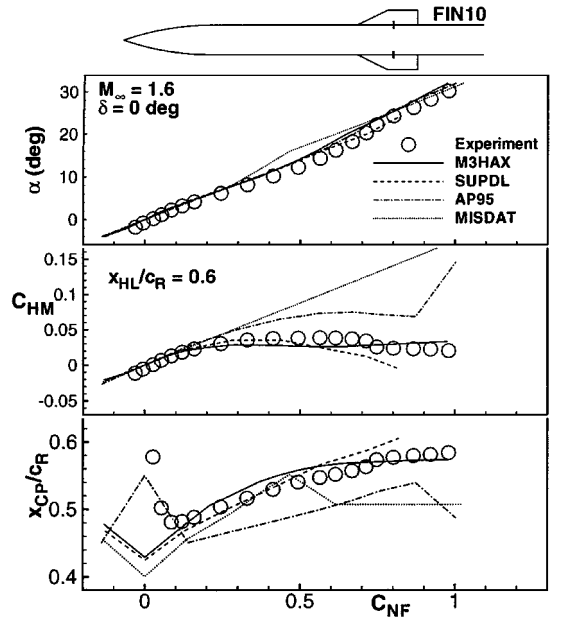

Fig. 18 FIN10 forces and moments; $M_\infty = 1.6$ and $\delta = 0$ deg.

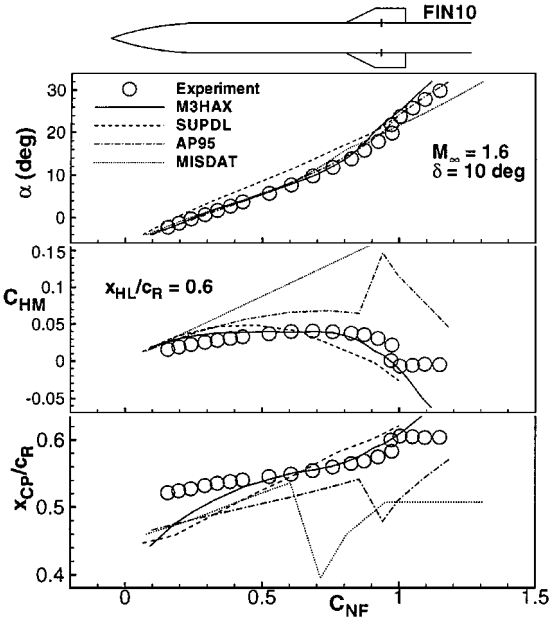

Fig. 19 FIN10 forces and moments; $M_\infty = 1.6$ and $\delta = 10$ deg.

variations than a higher aspect ratio fin and is more representative of future fins to be used in internal carriage configurations. Figures 18 and 19 show measured and predicted aerodynamic results for FIN10 at $M_\infty = 1.6$ for fin deflections of 0 and 10 deg, respectively. Angle of attack α, fin hinge-moment coefficient C_{HM}, and fin axial center of pressure X_{CP}/c_R are plotted as a function of the fin normal force coefficient C_{NF}. This choice of independent variable was taken because in this way the center-of-pressure locations tend to correlate best. Predictions are included from the M3HAX,[6] SUPDL,[8] AP95,[1] and Missile DATCOM[2] (MISDAT on graphs) codes.

To discern gap or unporting effects from fin force and moment data can be difficult. There are two primary gap effects that can be seen in the α vs C_{NF} curves for 0- and 10-deg fin deflection (Figs. 18 and 19). First, for the deflected fin the slope $\partial\alpha/\partial C_{NF}$ is less than that of the undeflected fin for $C_{NF} < 0.5$, which is actually an increase in the normal-force coefficient slope $\partial C_{NF}/\partial\alpha$. Second, there is a larger decrease in $\partial C_{NF}/\partial\alpha$ with an increasing angle of attack for the deflected fin. The increased $\partial C_{NF}/\partial\alpha$ slope of the deflected fin for $C_{NF} < 0.5$ is not an intuitive result. There should be a decrease in fin-body carryover effect and a decrease in the favorable body-upwash effect for the deflected fin. These effects can actually be seen in C_{NF} and can be estimated by comparing the $\alpha = 10$, $\delta = 0$ results to the $\alpha = 0$, $\delta = 10$ results: $C_{NF}(\alpha = 10, \delta = 0)$ is 0.41, and $C_{NF}(\alpha = 0, \delta = 10)$ is 0.25. Or, $\partial C_{NF}/\partial\alpha > \partial C_{NF}/\partial\delta$ because of the increased body upwash and increased fin-body carryover effects for the undeflected fin (no unporting). The larger decrease in $\partial C_{NF}/\partial\alpha$ for the deflected fin at higher angle of attack is caused by fin stall because the deflected fin is at a large angle of incidence and is subjected to unporting effects that may induce flow separation and stall. The increase in $\partial C_{NF}/\partial\alpha$ of the deflected fin for $C_{NF} < 0.5$ is not fully understood.

From the comparisons with experiment, one can see that all of the prediction methods estimate the fin normal force adequately for design. However, the SUPDL program underestimates C_{NF} for the deflected fin. Both the M3HAX and SUPDL codes estimate and characterize the hinge moment and the axial center-of-pressure location behavior well. The extensive correlations of vortex-free fin center-of-pressure location incorporated in the M3HAX code[6] from the Triservice fin-on-body data base,[12] and the use of the detailed vortex modeling including vortex effects on fin center of pressure, provide good agreement for this case. The panel method-based SUPDL[8] also includes detailed vortex modeling, which is necessary to estimate fin hinge moment and center-of-pressure location. For various reasons the AP95 and Missile DATCOM codes are not as successful in predicting the hinge moments and axial center-of-pressure locations for the undeflected and deflected cases. One reason is that both M3HAX and SUPDL include effects of upstream vorticity. In addition, the M3HAX code inherently includes nonlinearities associated with the Triservice fin-on-body database.

Rolling Moments Acting on Canards with Fixed Cant Angles

The NEARZEUS/ZEUSBL codes have been applied[17,31–34] to a range of configurations and supersonic flow conditions, from simple body-alone shapes at low supersonic Mach numbers to a waverider configuration at Mach 20. For this paper comparisons of measured (private communication, Stephen McIlwain, Shorts Missile Systems, Belfast, Northern Ireland, United Kingdom, 1997) and predicted rolling moment coefficients on a missile forebody with canards are presented. The configuration of interest, which consists of a missile forebody with canted delta-planform canards, is shown in Fig. 20. Wind-tunnel results were obtained at a freestream Mach number of 3.5 and several included angles of attack. Rolling moment data were obtained as a function of roll angle ϕ, where ϕ is measured relative to the horizontal and is positive for right wing down. Note that the canards are canted leading edge up at $\phi = 0$ deg with the starboard and port canards at different angles.

For the NEARZEUS calculations it is required that the flow everywhere be supersonic; however, there are obviously regions on the tip of the blunt nose where this condition is not met. Therefore,

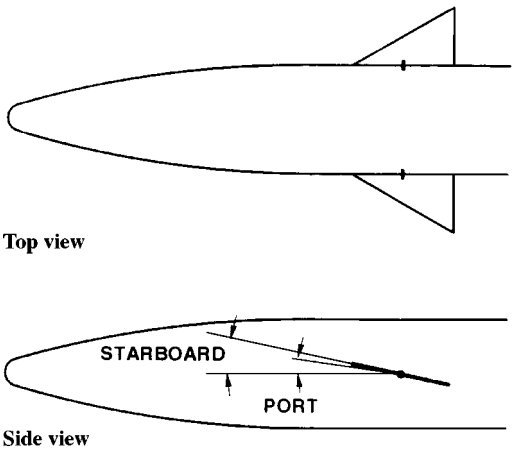

Fig. 20 Canard/forebody geometry.

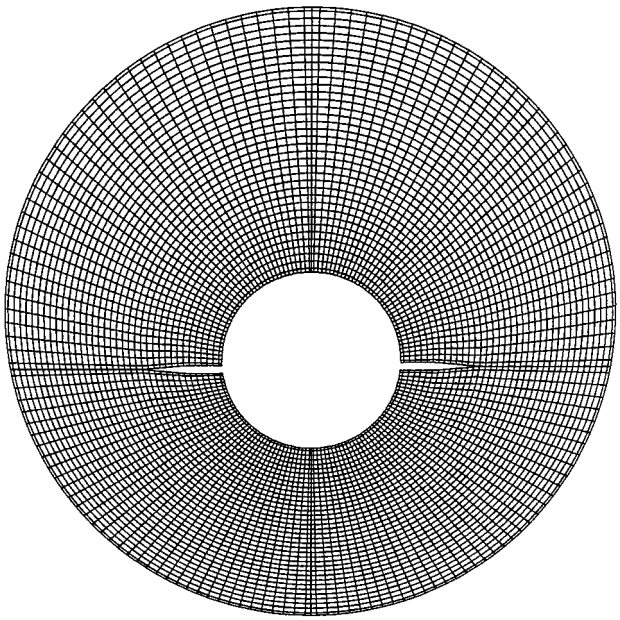

Fig. 21 Typical NEARZEUS grid layout in region of canards.

a blunt body solver is used,[35] which provides to the NEARZEUS code a starting plane solution at which the flow is everywhere supersonic. Next, a series of NEARZEUS calculations are carried out to obtain the overall forces and moments on the canard/forebody configuration. First, a NEARZEUS calculation is carried out for the nose region up to an axial station just ahead of the forwardmost canard leading edge. Then, the nose grid layout is converted to that to be used for the canards region. A slice showing the grid layout in the middle of the canards region is shown in Fig. 21. In this case the outer boundary of the grid layout is coincident with the bow shock. For all calculations the grid is made up of 36 radial cells and 144 circumferential cells. Finally, a NEARZEUS calculation is carried out for the canards region.

Comparisons of measured and predicted rolling moment coefficients at Mach number 3.5 are presented as a function of roll angle in Fig. 22 for total included angles (α_c) of 4 and 10 deg. The magnitude of the rolling moment has purposely been left off these plots because of the proprietary nature of the data; however, it can be reported that a negative rolling moment is produced at $\phi = 0$ deg, as would be expected from the starboard canard having a larger leading-edge up deflection angle than that of the port canard. These comparisons indicate excellent agreement between the measured and predicted results in regard to both the magnitude of the rolling moment coefficient and the variation with roll angle. As is shown in Fig. 22, the maximum negative rolling moment is reached near $\phi = 60$ deg, where the starboard canard is fully exposed to the windward flow and the port canard is partially shadowed by the body. At

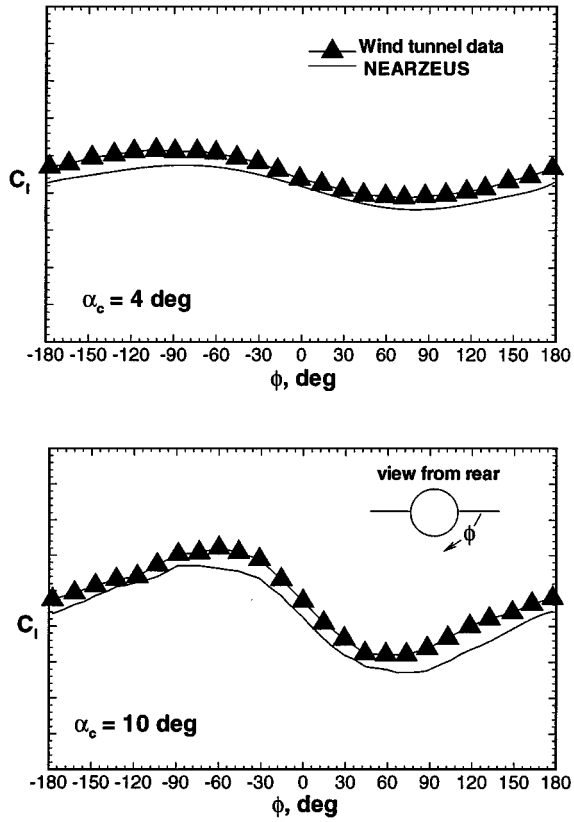

Fig. 22 Variation of rolling moment coefficient with roll angle on a canard-forebody; $M_\infty = 3.5$.

$\phi = \pm 180$ deg the configuration has been completely flipped over, and the difference in the loadings between the canards is seen to be approximately the same as that at $\phi = 0$ deg. As the rotation continues (from $\phi = -180$ to 0 deg), the starboard canard is increasingly in the shadow of the body, but the difference in loadings between the canards, as indicated by the rolling moment, is actually reduced compared to that at $\phi = 0$ and 180 deg. Peak values in rolling moment are indicated near $\phi = \pm 60$ deg.

Fin Planform Optimization

Many design studies have been performed utilizing the NEAR-developed optimization software, including fin planform optimizations, two-finned set optimizations, and body-shape optimizations. Results of fin planform optimization studies are presented here. The planform shapes described here have been tested in the wind tunnel as part of an Air Force SBIR Contract.[20] A total of six fin planforms were tested in the wind tunnel. The circular body of the wind-tunnel model was 5 in. in diameter, and its length was 36 in. Four of the fins had exposed spans of 3.61 in., and two had spans of 7.0 in. One fin of each span was a reference trapezoidal fin. These reference fins were used to start the optimization design studies. Fin performance is measured relative to the reference fins.

Figure 23 depicts small span fins designated FIN1 (reference) and FIN3 (optimized). Other fins tested are described in Ref. 20. The OPTMIS software was used to design FIN3 with FIN1 as the initial guess reference fin. The design objective was to minimize the fin axial center-of-pressure travel from subsonic to supersonic speeds over a realistic range of angle of attack. The objective can be restated to reduce the variation of axial center-of-pressure travel as a function of fin normal force. The design variables used for these cases were the fin leading- and trailing-edge shapes. The fin root chord and exposed span were fixed. The design variables used in the optimization studies were third-order Chebyshev polynomials describing the leading- and trailing-edge shapes.

Figure 23 compares measured and predicted results for FIN3 (optimized) and FIN1 (reference) for a fin deflection angle of 0 deg. The axial center of pressure is plotted as a function of the fin normal force coefficient (based on fin area). Predicted results are shown from the

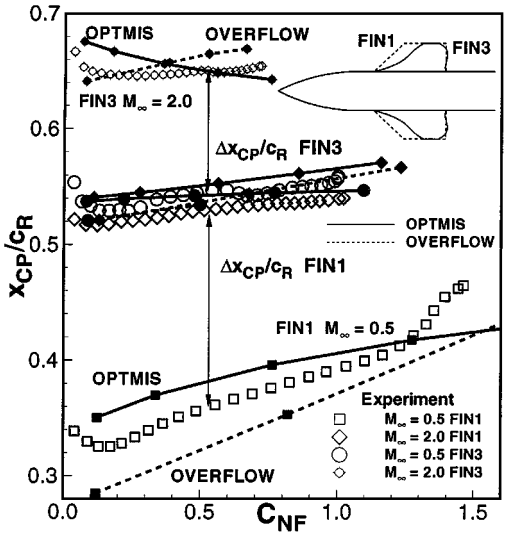

Fig. 23 X_{CP}/c_R **for reference fin FIN1 and optimized fin FIN3.**

OPTMIS code and the Navier–Stokes flow solver OVERFLOW.[36] The experiment, the design code OPTMIS, and the CFD results indicate that the optimized fin FIN3 has less center-of-pressure travel from subsonic to supersonic speeds and that the optimized fin has a flatter axial center-of-pressure variation with increasing fin normal force as compared to the reference fin. There is, in general, good agreement between the predictions and the experiment.

Concluding Remarks

This paper presents applications of a variety of missile aerodynamics prediction methods developed by and/or routinely used at NEAR: the experimental data-based M3HAX code, the panel method-based SUBDL/SUPDL codes, the modified linear theory VTXCHN code, and the Euler solver-based NEARZEUS code. Because these methods are easy to use and fast-running on workstations, they are considered engineering prediction methods. The applications include two different canard-tail missile configurations for which pitch-plane and lateral-directional aerodynamics are predicted and compared with subsonic and supersonic experimental data. Circular and chined cross-section body-alone cases are analyzed by the body vortex shedding VTXCHN code, and the results are compared with experimental data for high angle of attack with and without angle of sideslip. Pitch-plane aerodynamic characteristics are predicted for a nonconventional wing-body configuration using a combination of SUBDL and VTXCHN. The M3HAX, SUPDL, and other prediction methods are applied to assessing the effects of fin-body gap caused by deflection on the fin aerodynamic loads. Rolling moments as a function of roll angle are predicted by the NEARZEUS code and compared with experimental data for a canard-forebody configuration having two canard fins with fixed cant angles. Finally, examples are given of a fin planform optimization effort using the SUBDL/SUPDL methodology coupled with an optimization code. The design objective is to minimize axial center-of-pressure travel.

It is clear from the comparisons that any missile aerodynamics prediction method must include models for nonlinear flow phenomena such as vortical effects. To be really useful, missile aerodynamics predictions must be able to provide estimates of lateral directional aerodynamic characteristics related to asymmetric deflections and/or roll angles different from 0 or 45 deg. Some prediction methods do not have the capability or flexibility to generate results at arbitrary roll angles or to provide lateral directional aerodynamic characteristics. The missile designer/aerodynamicist has now been informed of a wide range of presently available aerodynamic prediction methods.

Acknowledgments

The development of the NEAR methodology described in this paper was originally supported by the Office of Naval Research, NASA Langley Research Center, Wright–Patterson Air Force Base, Naval Air Systems Command, Army Missile Command, and others. Further extensions and modifications were funded by the Naval Air Warfare Center, Weapons Division, China Lake, California, to provide aerodynamic support, with Ed Jeter as Technical Point of Contact. NEAR would like to thank Andy Sullivan and Fred Davis, WL/MNAV, Eglin Air Force Base, Florida, for supporting the fin planform optimization work under an SBIR effort. NEAR would also like to thank Stephen McIlwain, Short Missiles Systems, Belfast, Northern Ireland, United Kingdom, for his assistance in obtaining the canted canard comparisons between wind-tunnel data and NEARZEUS predictions.

References

[1]Moore, F., "Current Status and Future Plans of the Aeroprediction Code," AIAA Paper 97-2279, June 1997.

[2]Blake, W., "Missile DATCOM: 1997 Status and Future Plans," AIAA Paper 97-2280, June 1997.

[3]Perkins, S. C., Jr., Wardlaw, A. B., Priolo, F., and Baltakis, F., "NEARZEUS User Manual," Vol. I-Operational Instructions, Vol. II-Sample Cases, Vol. III-Boundary Layer Code ZEUSBL, Nielsen Engineering and Research, Inc., NEAR TR 459, Mountain View, CA, May 1996.

[4]Burns, K. A., Deters, K. J., Haley, C. P., and Kihlken, T. A., "Viscous Effects on Complex Configurations," McDonnell Douglas Aerospace, WL-TR-95-3060, St. Louis, MO, Aug. 1995.

[5]Mendenhall, M. R., and Perkins, S. C., Jr., "Computational Methodology for Maneuvering Aircraft at High Angles of Attack," Nielsen Engineering and Research, Inc., NEAR TR 508, Mountain View, CA, April 1996.

[6]Lesieutre, D. J., Love, J. F., and Dillenius, M. F. E., "High Angle of Attack Missile Aerodynamics Including Rotational Rates—Program M3HAX," AIAA Paper 96-3392, July 1996.

[7]Lesieutre, D. J., Dillenius, M. F. E., and Whittaker, C. H., "Program SUBSAL and Modified Subsonic Store Separation Program for Calculating NASTRAN Forces Acting on Missiles Attached to Subsonic Aircraft," Naval Air Warfare Center, Weapons Div., Rept. NAWCWPNS TM 7319, China Lake, CA, May 1992.

[8]Dillenius, M. F. E., Perkins, S. C., Jr., and Lesieutre, D. J., "Modified NWCDM-NSTRN and Supersonic Store Separation Programs for Calculating NASTRAN Forces Acting on Missiles Attached to Supersonic Aircraft," Naval Weapons Center, Rept. NWC TP 6834, China Lake, CA, Sept. 1987.

[9]Hegedus, M., Dillenius, M. F. E., and Love, J. F., "VTXCHN, Prediction Method For Subsonic Aerodynamics and Vortex Formation on Smooth and Chined Forebodies at High Alpha," AIAA Paper 97-0041, Jan. 1997.

[10]Dillenius, M. F. E., Lesieutre, D. J., Whittaker, C. H., and Lesieutre, T. O., "New Applications of Engineering-Level Missile Aerodynamics and Store Separation Prediction Methods," AIAA Paper 94-0028, Jan. 1994.

[11]Lesieutre, D. J., Dillenius, M. F. E., and Whittaker, C. H., "*M3F3CA* Aerodynamic Analysis for Finned Vehicles with Axisymmetric Bodies," Nielsen Engineering and Research, Inc., NEAR TR 424, Mountain View, CA, May 1991.

[12]Allen, J. M., Shaw, D. S., and Sawyer, W. C., "Analysis of Selected Data from the Triservice Missile Data Base," AIAA Paper 89-0478, Jan. 1989.

[13]Albright, A. E., Dixon, C. J., and Hegedus, M. C., "Modification and Validation of Conceptual Design Aerodynamic Prediction Method," NASA CR-4712, March 1996.

[14]Dillenius, M. F. E., Love, J. F., Hegedus, M. C., and Lesieutre, D. J., "Program STRLNCH for Simulating Missile Launch from a Maneuvering Parent Aircraft at Subsonic Speed," Nielsen Engineering and Research, Inc., NEAR TR 509, Mountain View, CA, Sept. 1996.

[15]Wardlaw, A. B., Jr., Baltakis, F. P., Martin, F. M., Priolo, F. J., and Jettmar, R. U., "Godunov's Method for Supersonic Tactical Missile Computations," AIAA Paper 85-1812, Aug. 1985.

[16]Wardlaw, A. B., Jr., and Davis, S. F., "A Second Order Godunov Method for Tactical Missiles," CP-412, AGARD, April 1986.

[17]Priolo, F. J., Wardlaw, A. B., Jr., and Kuhn, G. D., "High-Temperature Effects for Missile-Type Bodies Using the Euler Solver, ZEUS," AIAA Paper 91-3259, Sept. 1991.

[18]Wardlaw, A. B., Jr., and Baltakis, F. P., "An Integral Boundary Layer Procedure for Tactical Missiles," AIAA Paper 92-1024, Feb. 1992.

[19]Kwong, K., Suchsland, K., and Tong, H., "Momentum/Energy Integral Technique (MEIT) User's Manual," Accurex Corporation/Aerospace Systems Div., UM-78-86, Mountain View, CA, Feb. 1978.

[20]Lesieutre, D. J., Dillenius, M. F. E., and Lesieutre, T. O., "Multidisciplinary Design Optimization of Missile Configurations and Fin Planform for Improved Performance," AIAA Paper 98-4890, Sept. 1998.

[21]Powell, M. J. D., "An Efficient Method for Finding the Minimum of a Function of Several Variables Without Calculating Derivatives," *Computation Journal*, Vol. 7, 1964, pp. 155–162.

[22]Sargent, R. W. H., "Minimization Without Constraints, Optimization and Design," *Optimization and Design*, edited by M. Avriel, M. J. Rijckaert, and D. J. Wilde, Prentice–Hall, Upper Saddle River, NJ, 1973.

[23]Dillenius, M. F. E., Canning, T. N., Lesieutre, T. O., and McIntosh, S. C., "Aeroelastic Tailoring Procedure to Optimize Missile Fin Center of Pressure Location," AIAA Paper 92-0080, Jan. 1992.

[24]Fiacco, A. V., and McCormick, G. P., *Nonlinear Programming*, Wiley, New York, 1968.

[25]Brown, A. E., and Piper, E. M., "AIM9-L Wind Tunnel Test Report," Naval Weapons Center, NWC TN 4062-233 Rev. 1, China Lake, CA, Feb. 1974.

[26]Blair, A. B., Allen, J. M., and Hernandez, G., "Effect of Tail-Fin Span on Stability and Control Characteristics of a Canard-Controlled Missile at Supersonic Mach Numbers," NASA TP-2157, June 1983.

[27]"Tail Control Sparrow Wind Tunnel Test at NASA/Ames Research Center," Raytheon Co., Raytheon Rept. BR-9105, Final Rept., Bedford, MA, April 1976.

[28]Monta, W. J., "Supersonic Aerodynamic Characteristics of a Sparrow III Type Missile Model with Wing Controls and Comparison with Existing Tail-Control Results," NASA TP-1078, Nov. 1977.

[29]Guynn, M. D., "Evaluation of Two Discrete Vortex Based Forebody Aerodynamic Prediction Codes," *Proceedings of the Non-Linear Aero Prediction Methodology Workshop (Draft)*, edited by M. J. Logan, NASA Langley Research Center, Hampton, VA, 1994.

[30]Allen, J. M., Hemsch, M. J., Burns, K. A., and Deters, K. J., "Parametric Fin-Body and Fin-Alone Database on a Series of 12 Missile Fins," Proposed NASA TM, May 1996 (to be published).

[31]Wardlaw, A. B., Jr., and Priolo, F. J., "Applying the Zeus Code," U.S. Naval Surface Weapons Center, NSWC TR 86-508, White Oak, MD, Dec. 1986.

[32]Allen, J. M., Hernandez, G., and Lamb, M., "Body Surface Pressure Data on Two Monoplane-wing Missile Configurations with Elliptical Cross Sections at Mach 2.50," NASA TM-85645, Sept. 1983.

[33]Bibel, J. E., and Hardy, S. R., "Wind Tunnel Test Data of the High Performance Point Defense Missile (HPPDM) Obtained in the NASA Unitary Plan Wind Tunnel," U.S. Naval Surface Weapons Center, NAVSWC TR 90-475 (unpublished), Dahlgren, VA, Sept. 1990.

[34]Guard, F. L., and Schultz, H. D., "Preliminary Design and Experimental Investigation of the FDL-5A Unmanned High L/D Spacecraft, Part IV—Aerothermodynamics," U.S. Air Force Flight Dynamics Lab., AFFDL TR-68-24, Wright–Patterson AFB, OH, March 1968.

[35]Hsieh, T., and Priolo, F. J., "Generation of the Starting Plane Flowfield for Supersonic Flow over a Spherically Capped Body," U.S. Naval Surface Weapons Center, NSWC TR 84-484, White Oak, MD, May 1985.

[36]Buning, P. G., Chan, W. M., Renze, K. J., Sondak, D. L., Chiu, I. T., Slotnick, J. P., Gomez, R. J., Jespersen, D. C., Krist, S. E., and Rizk, Y. M., "OVERFLOW User's Manual—Version 1.6be," NASA Ames Research Center, Moffett Field, CA, Feb. 1996.

R. M. Cummings
Associate Editor